

## Feedback and rotational stabilization of resistive wall modes in ITER

Yueqiang Liu<sup>1</sup>, A. Bondeson<sup>1,+</sup>, M.S. Chu<sup>2</sup>, J-Y. Favez<sup>3</sup>, Y. Gribov<sup>4</sup>, M. Gryaznevich<sup>5</sup>, T.C. Hender<sup>5</sup>, D.F. Howell<sup>5</sup>, R.J. La Haye<sup>2</sup>, J.B. Lister<sup>3</sup>

<sup>1</sup> Department of Electromagnetics, EURATOM/VR Fusion Association, Chalmers University of Technology, Göteborg, Sweden

<sup>2</sup> General Atomics, San Diego, CA, USA

<sup>3</sup> CRPP, Ecole Polytechnique Fédérale de Lausanne, Switzerland

<sup>4</sup> Physics Unit, ITER Naka Joint Work Site, Naka, Ibaraki, Japan

<sup>5</sup> Euratom/UKAEA Fusion Association, Culham Science Centre, Abingdon, UK

<sup>+</sup> deceased

e-mail contact of main author: elfliu@elmagn.chalmers.se

**Abstract.** Different models have been introduced in the stability code MARS-F in order to study the damping effect of resistive wall modes (RWM) in rotating plasmas. Benchmark of MARS-F calculations with RWM experiments on JET and D3D indicates that the semi-kinetic damping model is a good candidate for explaining the damping mechanisms. Based on these results, the critical rotation speeds required for RWM stabilization in an advanced ITER scenario are predicted. Active feedback control of the  $n = 1$  RWM in ITER is also studied using the MARS-F code.

### 1. Introduction

One of the major limiting factors for achieving high beta in advanced tokamaks is the onset of resistive wall modes (RWM). These are usually pressure driven, low  $n$ , external kink modes, whose growth rates are greatly suppressed by surrounding conducting walls. The modes become unstable as soon as the plasma pressure exceeds the no-wall ideal limit, with a growth time of order the wall eddy current decay time. Therefore, the RWM must be stabilized in order to achieve steady state operations, with high plasma pressures, in the ITER advanced scenarios.

Two possible approaches have been proposed to stabilize the RWM: the toroidal plasma rotation and active feedback. It has been shown, in both theory [1] and experiments in DIII-D [2, 3], that the RWM can be completely stabilized by plasma rotation, provided that the rotation speed exceeds some critical value, which is typically a few percent of the Alfvén frequency. Since it is probably not possible to maintain a very high speed rotation for ITER plasmas, the critical rotation speed for RWM stabilization in ITER is an important issue. Calculations using MARS-F code [5] show that the critical rotation depends sensitively on the damping models. This paper reports detailed benchmarking of the damping models against the experimental results in JET and DIII-D. These benchmark results allow us to choose a good damping model for the ITER prediction.

The possibility of stabilizing the RWM using feedback control has been actively exploited during the recent years, both in theory and experiments. In previous papers, e.g. [5, 6], we have shown that active stabilization for tokamaks works best when sensors for the poloidal field are placed inside the first wall. Robust stabilization of pressure-driven  $n = 1$  kinks can be achieved, by using a single array of coils, located poloidally at the outboard midplane, where the modes balloon [6]. Recently MARS-F has been used to study active control of RWM

for the present ITER design [7]. This paper studies the possibility of improving the feedback control for ITER plasmas, by choosing better sensor signals, and by using internal feedback coils, as opposed to the external coils in the present ITER design.

## 2. Rotational stabilization

**2.1 Damping models** A key issue in understanding the physics of RWM in a rotating plasma is the damping mechanism. It was suggested some time ago [1] and verified with recent experiments [3], that besides the Alfvén continuum damping, the ion Landau damping also plays an important role in suppressing the mode.

In the MARS-F code, the ion Landau damping is modeled in two ways. One is the parallel sound wave damping, where a viscosity force,

$$\vec{F}_{\text{visc}} = -\kappa_{\parallel} |k_{\parallel}| v_{th,i} \rho \vec{v}_{\parallel}, \quad (1)$$

for each (m,n)-component of the helical perturbations, is added to the momentum equation (in the single fluid MHD setup) along the parallel motion. In Eq. (1),  $k_{\parallel} \equiv (m/q - n)/R$  is the parallel wave number,  $v_{th,i}$  is the ion thermal velocity,  $\rho$  is the mass density, and  $\vec{v}_{\parallel}$  is the perturbed parallel velocity of the plasma. The drawback of this model is the presence of an adjustable parameter  $\kappa_{\parallel}$ .

The other model follows a simplified drift-kinetic large-aspect-ratio analysis [8], where the kinetic energy perturbations are computed taking into account the contributions from both circulating and trapped particles.

$$\Delta W_T = \frac{1}{2} \sum_{m'} \int d^3x \int_{trapped} d\Gamma \left( -\frac{\partial f}{\partial E} \right) \frac{\omega}{\omega + m' \omega_b} | \langle \exp(j\chi_{m'}) H \rangle |^2 \quad (2)$$

$$\Delta W_C = \frac{1}{2} \sum_{m'} \int d^3x \int_{circ} d\Gamma \left( -\frac{\partial f}{\partial E} \right) \frac{\omega}{\omega - (nq - m') \omega_t} | \langle \exp(j\chi_{m'}) H \rangle |^2. \quad (3)$$

In Eq. (2)-(3),  $f$  is the Maxwellian distribution,  $E$  is the particle energy,  $n$  the toroidal mode number,  $m'$  the bounce harmonics,  $\omega_b$  the bounce frequency of the trapped particles, and  $\omega_t$  the transit frequency of the passing particles.  $\omega$  is the real frequency of the mode with respect to the plasma. For RWM studies, we use the plasma rotation frequency for  $\omega$ . The quantities  $\chi'_m$  are defined as phase factors for passing and trapped particles, respectively. The quantity  $H$  is the perturbation of a particle's energy, which is determined by the perturbation of the magnetic field strength together with the field line curvature.

The imaginary part (responsible for damping) of the kinetic  $\Delta W = \Delta W_T + \Delta W_C$  is evaluated and the equivalent damping force  $F_{\text{diss}}$  is computed via the relation

$$j \text{Im}(\Delta W_C + \Delta W_T) = -\frac{1}{2} \int \vec{F}_{\text{diss}} \cdot \vec{\xi}_{\perp}^* d^3x. \quad (4)$$

As shown in Eq. (4), the added damping force acts on the perpendicular motion. Due to the toroidal coupling, the  $m$  component of the field perturbation  $\vec{b}$  couples to the  $m \pm 1$  components of the parallel motion. This coupling makes the Landau damping rather nonlocal. For example, even at  $\omega \sim 0.02\omega_A$ , the momentum transfer is spread out over entire plasma. This explains the 'strong' damping effect from the kinetic model, as will be shown in the following sections.

The present kinetic damping model neglects the effects of finite diamagnetic and gyrocenter drift frequencies ( $\omega_* = \omega_D = 0$ ). These effects may be of importance for more appropriate modeling, and will be included into the MARS-F code in the future.

**2.2 Critical rotation velocity** Using two damping models, we computed the critical rotation speeds for two series of equilibria based on JET shot #62366 and DIII-D shot #109174. The chosen JET equilibria have  $q_{95}$  around 4.8, and the DIII-D equilibria have  $q_{95}$  around 3.6. Shown in Fig.1(a-b) is the comparison of the MARS-F calculations with the experimental data. The critical rotation is plotted against the plasma pressure, which is described by a parameter  $C_\beta \equiv (\beta_N - \beta_N^{\text{no-wall}})/(\beta_N^{\text{ideal-wall}} - \beta_N^{\text{no-wall}})$ .

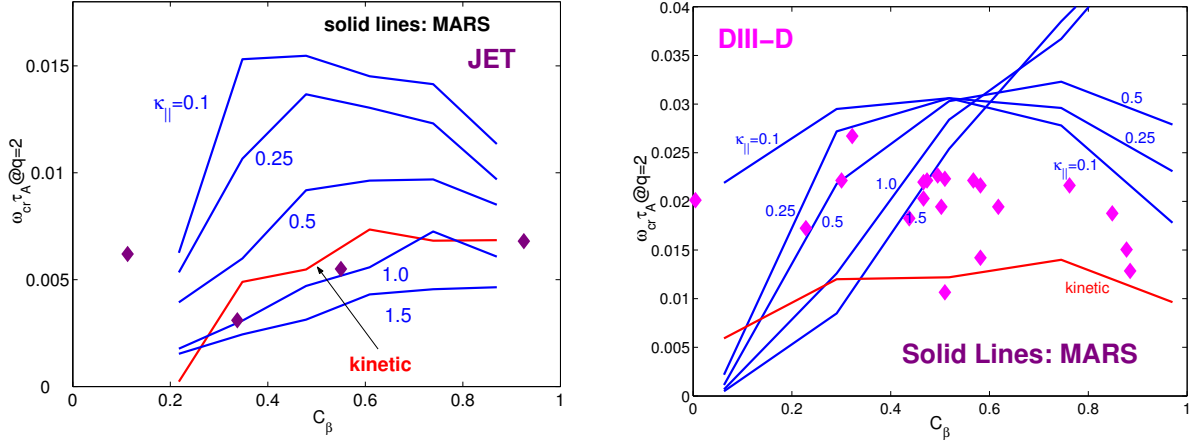


FIG.1. The critical rotation frequency at  $q = 2$  surface, normalized by Alfvén frequency, versus the plasma pressure characterized by  $C_\beta \equiv (\beta_N - \beta_N^{\text{no-wall}})/(\beta_N^{\text{ideal-wall}} - \beta_N^{\text{no-wall}})$ . Plotted are experimental data (dots) and the MARS-F results (solid curves) with parallel sound wave damping and semi-kinetic damping models, (a) - for JET, (b) - for DIII-D.

The kinetic damping, as well as the sound wave damping with  $\kappa_{||} = 1 - 1.5$ , gives good prediction for JET plasmas, when compared with initial experimental results [4]. For DIII-D, the kinetic damping model underestimates the critical rotation by about 40%, whereas the sound wave damping model with  $\kappa_{||} = 0.1$  overestimates the critical rotation by about 40%. It should be noted that for both JET and DIII-D, the dependence of critical rotation on the plasma pressure is not sensitive. Such behavior is correctly recovered by the kinetic damping model.

Figure 1 also shows that the critical rotation in JET is generally 2-4 times smaller than that in DIII-D. Such difference is observed in both experimental data and in MARS-F calculations. In order to resolve the possible cause for this, we made calculations for a series of equilibria varying from JET to DIII-D. Shown in Fig. 2 is the computed critical rotation for four equilibria, using the kinetic damping model. Eq#1 is a JET equilibrium reconstructed from shot #62653 at 46.68s, with the JET plasma rotation profile, eq#4 a DIII-D equilibrium from shot #109174, with the DIII-D rotation profile. Eq#2 is the same JET equilibrium but with DIII-D rotation profile. Eq#3 has the current density (and pressure) profile from JET, but the plasma and wall shapes as well as the rotation profile from DIII-D. For the specific cases studied here, the plasma rotation profile has much less influence on the critical rotation, than the plasma and wall shapes. The wall is relatively farther away in JET and the spread in beta between the no

wall and ideal wall limits is smaller in JET than in DIII-D. The current density profiles (via the  $q$ -profiles) also have significant influence on the critical rotation. Note that in this study, both the JET and DIII-D equilibria have similar  $q_{95}$ , which is about 3.4 for JET and about 3.6 for DIII-D. For the 'intermediate' equilibria, we keep the  $q_{95}$  to be 3.4 by scaling the total plasma current. For all four cases, the  $C_\beta$  values are approximately 0.5. It should be pointed out that the measured critical rotation for this JET shot is about twice larger than the value computed by MARS-F. Such a discrepancy, as well as the discrepancy observed for DIII-D modeling, indicates that further improvement of the damping models is necessary.

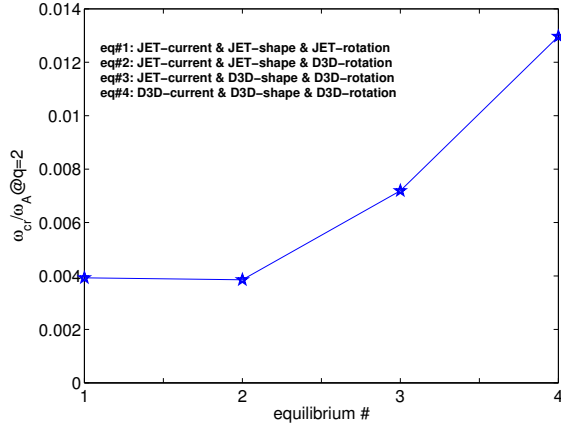


FIG.2. The critical rotation velocity computed for a series of equilibria varying from JET to DIII-D. The  $C_\beta$  and  $q_{95}$  are kept approximately the same for all equilibria.

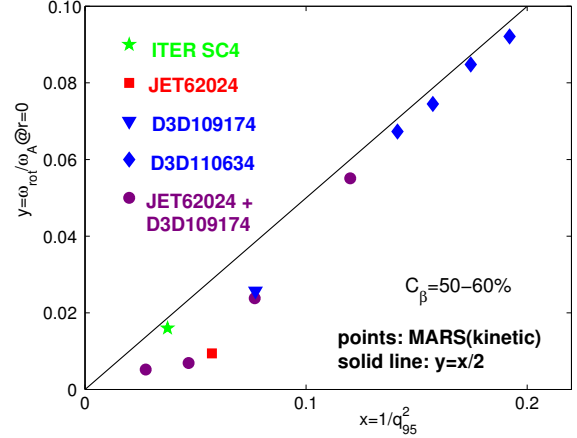


FIG.3. The critical rotation velocity computed for various equilibria using MARS-F with the kinetic damping model (dots). Plotted is the critical rotation frequency at the plasma center versus  $q_{95}$ .

For fixed equilibrium profiles and shapes, we found that the critical rotation has strong dependence on  $q_{95}$ . Figure 3 collects all the computed data for various equilibria from JET, DIII-D and ITER. For all the equilibria, The plasma pressure is scaled to  $C_\beta = 50 - 60\%$ . For a given experimental shot (i.e., the equilibrium current and pressure profiles, the rotation profile, the plasma and wall shapes are fixed),  $q_{95}$  is scaled by varying the total plasma current.

As shown in Fig.3, the critical rotation velocity generally increases with decreasing  $q_{95}$ . This indicates that, at high- $q$  discharges, the damping from the plasma edge may also be important for the RWM stabilization. For a fixed shot, the scaling is rather linear with respect to  $1/q_{95}^2$ , which agrees with the theory [8]. Of course, the critical rotation varies between different machines, as shown by Fig.2. Nevertheless, the scaling shown in Fig. 3 is in favor of high- $q$  equilibria with high bootstrap fraction.

**2.3 Resonant field amplification** Resonant field amplification (RFA) has been extensively exploited in DIII-D [9] and JET [4] experiments. These experiments can be viewed as MHD spectroscopy for rotationally stabilized RWM. Hence they also offer an excellent benchmark for the damping models.

We have pursued a systematic analysis of RFA experiments in JET using MARS-F [10, 4]. This analysis shows that (1) the computed amplitude and phase of the field amplification depend sensitively on the damping models used in MARS-F; (2) kinetic damping gives reason-

able agreement with the experimental data, for both internal and external saddle coils, with excitation currents in the form of both DC pulses and standing waves.

As an example, we show, in Fig.4, the computed total response of the plasma and the ewall to the applied error field from internal saddle coils. We plot in the complex plane the amplified field excited by traveling waves with various frequencies. The response is normalized by the vacuum field produced by a DC current. For comparison, the vacuum response (i.e. without plasma) of the conducting wall is also plotted. The computed results (denoted by circles) are approximated by second order rational functions (solid lines)

$$P_{\text{RFA}}(j\omega_c) = \frac{1.008 + j0.535}{j\omega_c + 0.884 - j0.281} + \frac{0.045 + j0.031}{j\omega_c + 0.176}, \quad (5)$$

$$P_{\text{VACUUM}}(j\omega_c) = \frac{0.911}{j\omega_c + 1} + \frac{0.021}{j\omega_c + 0.164}, \quad (6)$$

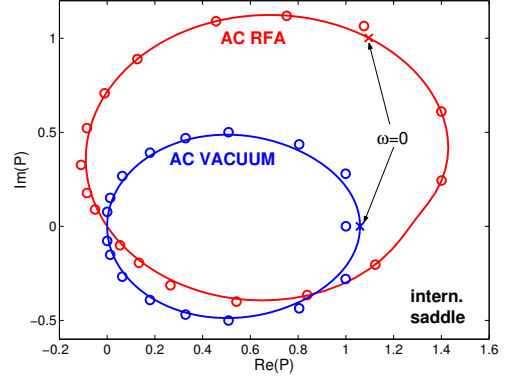


FIG.4. The MARS-F computed plasma response to traveling waves launched by internal saddle coils in JET.

where  $\omega_c$  is the traveling wave frequency normalized by the wall time. Figure 4 and Eqs.(5)-(6) show that the internal saddle coils cause a significant modification of the field even at the sensor position.

**2.4 ITER prediction** The benchmark study with JET and DIII-D experiments on critical plasma rotation and RFA indicates that the kinetic damping can be a good candidate for describing the damping physics for RWM. This allows us, with certain confidence, to predict the critical rotation for the RWM stabilization in ITER plasmas.

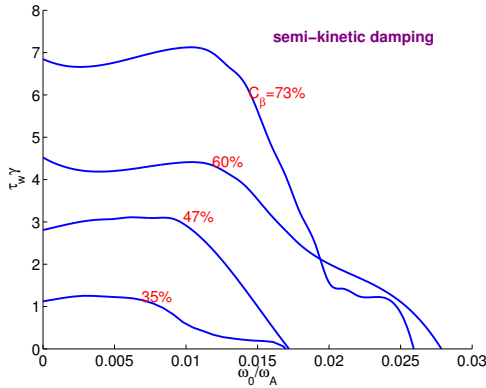


FIG.5. The computed growth rates of the RWM in ITER advanced scenario-4 for various plasma pressures. The semi-kinetic damping model is used.

We consider a steady state scenario for ITER (Scenario-4 from the ITER design) [7]. Figure 5 shows the computed growth rates of the  $n = 1$  RWM in the rotating ITER plasma, with increasing the rotation amplitude and fixing the rotation profile predicted by ASTRA code. The critical rotation frequency, predicted by the kinetic damping model, varies between 1.5-3% $\omega_A$  at the plasma center. Since the predicted (by ASTRA transport calculations) ITER plasma rotation is less than 2% $\omega_A$  at the plasma center, we conclude that rotational stabilization alone may not be robust for ITER plasmas. And active control of the RWM may be required.

### 3. Feedback stabilization

**3.1 Choice of feedback logic** For feedback control of ITER plasmas, we choose so-called voltage-to-voltage control

$$V_f = -KV_s,$$

where  $K$  is the controller. The voltage of the feedback coil ( $V_f$ ) and sensor loop ( $V_s$ ) are defined as

$$V_f = \frac{d\psi_f}{dt}, \quad V_s = \frac{L_f}{M_{sf}} \frac{d\psi_s}{dt},$$

where  $\psi_f$  is the flux through the feedback coil,  $\psi_s$  the flux through the sensor loop,  $L_f$  the self-inductance of the feedback coil, and  $M_{sf}$  the mutual inductance between the feedback and sensor coils. The resistance of the feedback coil is neglected since ITER has superconducting coils.

We introduce two transfer functions that completely describe the plasma response from the MHD calculations

$$P_1 = \frac{\psi_s}{M_{sf} I_f}, \quad P_2 = \frac{\psi_f}{L_f I_f}.$$

The total plasma response is thus determined by the transfer function  $P = P_1/P_2$ . The feedback coil from the present ITER design is rather far from the plasma (at radial distance of about  $3a$ , where  $a$  the plasma minor radius). As a consequence,  $P_2$  is typically close to 1.

**3.2 Choice of sensors** As has been pointed out earlier [11, 5], feedback stabilization of the RWM is sensitive to the choice of sensor signals. A good choice is the poloidal field component inside the vacuum wall at the outboard midplane [5]. This is denoted as internal poloidal sensors. Other possibilities are external poloidal sensors (i.e. poloidal sensor outside the wall), radial sensors (typically on the wall), radial sensors with compensation of the vacuum coil fields, and the combinations of these sensors. Quite often, the best choice turns out to be internal poloidal sensors alone. We illustrate this by studying a feedback system for a cylindrical plasma with the current density profile as a step function. In this case the transfer function  $P$ , including all poloidal harmonics, can be computed analytically [12] for all types of sensor signals. Let us denote the corresponding transfer functions as  $P_r, P_{p-}, P_{p+}, P_c$  for radial, internal poloidal, external poloidal sensors and for vacuum coils without the plasma but with the wall, respectively.

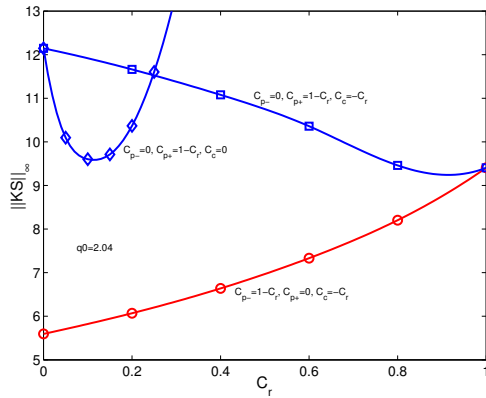


FIG.6. Controller optimization for various combinations of sensor signals. Results are obtained for a cylindrical plasma.

We define  $P_{\text{tot}} \equiv C_r P_r + C_{p-} P_{p-} + C_{p+} P_{p+} + C_c P_c$  as the transfer function for combined sensors, and minimize the control activity (approximately a measure of the feedback gain)  $\|KS\|_\infty \equiv \sup_{\omega} |K(j\omega)/(1 + K(j\omega)P_{\text{tot}}(j\omega))|$  with respect to a PD controller  $K(s) = K_p(1 + T_d s)/(1 + T_d s/\xi)$ , where  $\omega$  is the real frequency,  $s$  the Laplace transform variable, and  $K_p, T_d, \xi$  controller parameters that we optimize. Figure 6 shows the minimized  $\|KS\|_\infty$  versus parameter  $C_r$ , for three interesting combinations of the sensor signals. The best result is achieved by choosing  $C_{p-} = 1, C_r = C_{p+} = C_c = 0$ , i.e. by using only internal poloidal sensors. For feedback study of the RWM in ITER, we consider mainly internal poloidal sensors. In addition, a compensation scheme for such sensors is also proposed as shown in Section 3.4.

**3.3 Choice of feedback coils** The present ITER design uses the side correction coils for the RWM feedback control. These are superconducting coils, external to the ITER walls, with three pairs of toroidally opposite coils connected to produce the  $n = 1$  magnetic field.

Using MARS-F, we compute the transfer functions  $P_1$  for the designed equilibria in ITER Scenario-4, using internal poloidal sensors for feedback. These functions are then approximated (in frequency domain) with 2- or 3-pole rational functions. Shown in Fig. 7(a) are the transfer functions  $P_1(j\omega)$  in the complex plane for real frequencies  $\omega$  and for various plasma pressures. The closed-loop system will be stable, if the open-loop curve for  $K(j\omega)P_1(j\omega)$  (shown in Fig. 7 for a proportional gain  $K = 1$ ) encircles -1 once counterclock-wise. One can see that with proportional gains, the RWM can be stabilized for  $C_\beta$  value up to 60%. By adding appropriate derivative action, the mode can be stabilized even for higher pressures. These results are obtained by assuming an ideal amplifier for the feedback system.

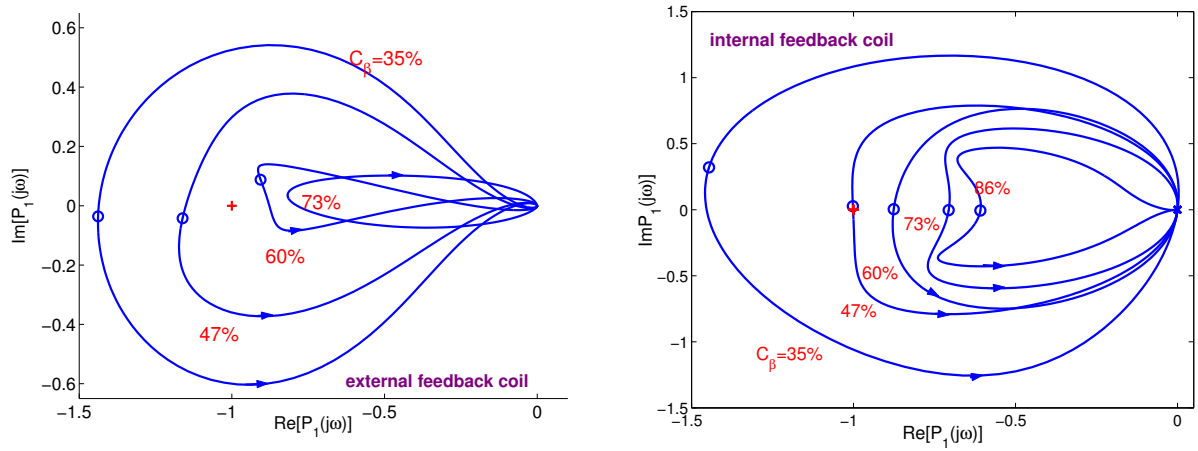


FIG.7. The transfer functions  $P_1(j\omega)$ , for real frequencies  $\omega$ , plotted in the complex plane for various plasma pressures for (a) external feedback coils in the ITER design, and (b) assumed internal feedback coils.

Figure 7(b) shows the computed transfer functions  $P_1(j\omega)$  if we move the feedback coils just inside the ITER inner wall. As expected, the control becomes much easier with internal feedback coils. A large enough proportional gain in this case stabilizes the RWM for  $C_\beta$  close to 1 (the ideal wall limit). Also, the performance of the control is better because of the larger phase of  $P_1(j\omega)$ .

**3.4 Control optimization for ITER** As shown in Fig. 7, the present design of feedback coils allow stabilization of the  $n = 1$  RWM up to  $C_\beta = 60\%$  using internal poloidal sensors and only proportional gains. Better results can be achieved by using optimally tuned PID controllers and improved sensor signals, as shown by Fig. 8. We choose a PID controller  $K(s) = (K_p + K_i/s)(1 + T_d s)/(1 + T_d s/\xi)$ , and optimize the four parameters  $\{K_p, K_i, T_d, \xi\}$  to achieve minimum peak voltage for a reference event where the controller is turned on after the field reaches 1.5 mT, subject to constraints on stability parameter  $J_S \equiv \|1/(1 + K(j\omega)P_1(j\omega))\|_\infty$  and the settling time  $\tau_{\text{set}}$ . In Fig. 8, the maximal voltage is plotted against  $C_\beta$ , for three sets of constraints, corresponding to three curves with 'o'.



With the design voltage limit of 300 V/turn for the amplifier, the RWM can be controlled with good performance ( $J_S = 2, \tau_{\text{set}}/\tau_w = 1$ ) for  $C_\beta \leq 65\%$ , and with moderate performance ( $J_S = 2.5, \tau_{\text{set}}/\tau_w = 2$ ) for  $C_\beta < 70\%$ . The peak voltage can be further decreased if we use the internal poloidal sensor signals compensated by a signal  $P_c(s) = T_{d2}/(s + \xi_2)$ , where parameters  $T_{d2}$  and  $\xi_2$  are optimally chosen and are the same for all pressures. The results are presented by three curves with '+' in Fig. 8. Within the voltage limit of 300 V/turn, the RWM can be stabilized, with good performance, up to  $C_\beta > 80\%$ .

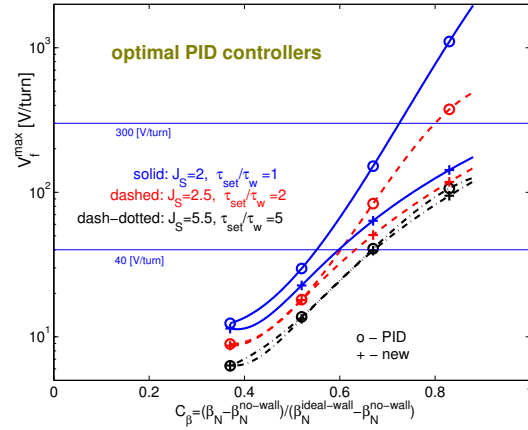


FIG.8. The maximum voltage required to stabilize the RWM versus the plasma pressure. The ITER design limit for the power amplifier is 300 V/turn.

#### 4. Conclusions

Two damping models have been benchmarked against the present experimental data for RWM study. The semi-kinetic damping model gives reasonable results for both critical plasma rotation required for the RWM stabilization, and the RFA experiments. Such a model predicts that the critical rotation frequency for stabilizing the  $n = 1$  RWM in ITER is about  $1.5\text{-}3\%\omega_A$  at the plasma center. Further improvement of this model is needed for better prediction. With the present coil design in ITER for feedback control, it is possible to stabilize the  $n = 1$  RWM for plasma pressures up to 80% between the no-wall and ideal-wall limits, using optimally tuned PID controllers and optimally compensated internal poloidal sensor signals. The control can be further improved by using internal feedback coils. Finally, more robust stabilization of the RWM in ITER is possible by combining feedback and plasma rotation [7].

**Acknowledgments** This work was conducted under the European Fusion Development Agreement and partly funded by EURATOM and by VR.

#### Reference

- [1] Bondeson, A., Ward, D.J., Phys. Rev. Lett. **72** (1994) 2709.
- [2] Garofalo A.M., et al, Phys. Plasmas **9** (2002) 1997.
- [3] La Haye R.J., et al, "Scaling of the Critical Plasma Rotation for Stabilization of the  $n = 1$  Resistive Wall Mode (Ideal Kink) in the DIII D Tokamak", Nucl. Fusion, (submitted).
- [4] Hender T.C., et al, "Resistive Wall Mode Studies in JET", this conference.
- [5] Liu Y.Q., et al., Phys. Plasmas **7** (2000) 3681.
- [6] Liu Y.Q., et al, Nucl. Fusion **44** 77 (2004).
- [7] Liu Y.Q., et al, Nucl. Fusion **44** 232 (2004).
- [8] Bondeson A. and Chu M.S., Phys. Plasmas **3** 3013 (1996).
- [9] Garofalo A.M., et al, Phys Plasmas **10**, 4776 (2003).
- [10] Liu Y.Q., et al, "Modeling of Resistive Wall Mode Experiments in JET", Preceeding of 30th EPS Conference on Plasma Phys. and Contr. Fusion, Imperial College, UK, 2004.
- [11] Liu Y.Q. and Bondeson A., Phys. Rev. Lett. **84** (2000) 907.
- [12] Bondeson A., et al., Nucl. Fusion **42** (2002) 768.